Observing ozone chemistry in an occupied residence

Yingjun Liu[a,b,c,1], Pawel K. Misztal[c,2], Caleb Arata[d], Charles J. Weschler[e,f], William W Nazaroff[g], and Allen H. Goldstein[c,g]

[a]State Key Joint Laboratory of Environmental Simulation and Pollution Control, College of Environmental Sciences and Engineering, Peking University, 100871 Beijing, China; [b]Beijing Innovation Center for Engineering Science and Advanced Technology, Peking University, 100871 Beijing, China; [c]Department of Environmental Science, Policy, and Management, University of California, Berkeley, CA 94720; [d]Department of Chemistry, University of California, Berkeley, CA 94720; [e]Environmental and Occupational Health Sciences Institute, Rutgers University, Piscataway, NJ 08854; [f]International Centre for Indoor Environment and Energy, Technical University of Denmark, Lyngby 2800, Denmark; and [g]Department of Civil and Environmental Engineering, University of California, Berkeley, CA 94720

Edited by John H. Seinfeld, California Institute of Technology, Pasadena, CA, and approved December 1, 2020 (received for review September 2, 2020)

Outdoor ozone transported indoors initiates oxidative chemistry, forming volatile organic products. The influence of ozone chemistry on indoor air composition has not been directly quantified in normally occupied residences. Here, we explore indoor ozone chemistry in a house in California with two adult inhabitants. We utilize space- and time-resolved measurements of ozone and volatile organic compounds (VOCs) acquired over an 8-wk summer campaign. Despite overall low indoor ozone concentrations (mean value of 4.3 ppb) and a relatively low indoor ozone decay constant (1.3 h^{-1}), we identified multiple VOCs exhibiting clear contributions from ozone-initiated chemistry indoors. These chemicals include 6-methyl-5-hepten-2-one (6-MHO), 4-oxopentanal (4-OPA), nonenal, and C8-C12 saturated aldehydes, which are among the commonly reported products from laboratory studies of ozone interactions with indoor surfaces and with human skin lipids. These VOCs together accounted for ≥12% molecular yield with respect to house-wide consumed ozone, with the highest net product yield for nonanal (≥3.5%), followed by 6-MHO (2.7%) and 4-OPA (2.6%). Although 6-MHO and 4-OPA are prominent ozonolysis products of skin lipids (specifically squalene), ozone reaction with the body envelopes of the two occupants in this house are insufficient to explain the observed yields. Relatedly, we observed that ozone-driven chemistry continued to produce 6-MHO and 4-OPA even after the occupants had been away from the house for 5 d. These observations provide evidence that skin lipids transferred to indoor surfaces made substantial contributions to ozone reactivity in the studied house.

ozonolysis | indoor | residential | squalene | exposure

Outdoor air containing ozone (O_3) penetrates into indoor environments, including residences, workplaces, and schools. Ozone undergoes fast reactions indoors; its characteristic lifetime is typically a few tens of minutes (1, 2). Reactions are thought mainly to occur on the large surface area in indoor environments (3), which ubiquitously contain reactive species (4, 5). Indoor ozone chemistry reduces indoor ozone concentrations and forms a spectrum of oxidation products, many of which are volatile (6). Emerging evidence suggests that indoor exposure to the mixture of ozone and its oxidation products contributes to epidemiologically determined associations between outdoor ozone concentrations and morbidity and mortality (3, 7).

Previous studies of indoor air chemistry mainly focused on investigating ozone reactions with individual indoor surfaces along with consequent release of secondary products. Studied surfaces include building materials and furnishings, such as carpet, wall coverings, ceiling tiles, wood boards, and glass (8–11), as well as human skin, hair, and clothing (12–14). Observed volatile products include C1-C13 carbonyls, dicarbonyls, and hydroxycarbonyls among other oxygenated compounds. Product yields vary broadly, influenced by factors such as type and age of surface materials (11, 15) and soiling (8, 13, 16, 17). Skin oil lipids, characterized by a high proportion of squalene ($C_{30}H_{50}$), are particularly important indoor ozone reactants (14). They are present on skin, hair, and worn clothing of human occupants. They can also be transferred to other surfaces such as bedding, furniture, and flooring via desquamation and by direct physical contact (18). Major volatile products of squalene ozonolysis include 4-oxopentanal (4-OPA), 6-methyl-5-hepten-2-one (6-MHO), and geranylacetone.

Past research targeting specific indoor materials and surfaces demonstrates important features of indoor surface ozone chemistry; however, these studies are insufficient for evaluating the contribution of ozone chemistry to the composition of dynamically changing indoor environments and hence to occupants' exposure (19). First, there can be myriad sources for indoor air pollutants in addition to ozone chemistry (20). Because ozone chemistry can produce a particular compound does not imply that it contributes meaningfully to the indoor concentration of that compound. Second, occupants might dynamically alter indoor ozone reactivity via their time-dependent presence indoors as well as their intended and unintended activities such as desquamation, transferring skin oils to surfaces by direct contact, cooking (e.g., surface soiling by the deposition of fatty acids in cooking oils and foods), and cleaning (e.g., with products that contain ozone-reactive terpenoids). Indoor studies in densely occupied spaces, including in two classrooms, a

Significance

It has been suggested that indoor exposure to ozone oxidation products contributes materially to the apparent associations between outdoor ozone concentration and morbidity and mortality. Our current understanding of indoor ozone chemistry derives mainly from studies with test surfaces under controlled conditions. Little is known about the overall impact of ozone chemistry on air composition in dynamically changing indoor residential environments. The results presented here reflect a quantitative characterization of overall indoor ozone chemistry in a normally occupied home. Findings reveal a strong influence of off-body skin lipids on indoor ozone chemistry. Being able to elucidate indoor air pollutants derived from ozone chemistry facilitates the investigation of causal links between outdoor ozone concentrations and adverse health effects.

Author contributions: Y.L., P.K.M., C.A., W.W.N., and A.H.G. designed research; Y.L., P.K.M., and C.A. performed research; Y.L., C.J.W., W.W.N., and A.H.G. analyzed data; and Y.L. wrote the paper.

The authors declare no competing interest.

This article is a PNAS Direct Submission.

[1]To whom correspondence may be addressed. Email: yingjun.liu@pku.edu.cn.

[2]Present address: Department of Civil, Architectural and Environmental Engineering, University of Texas at Austin, Austin, TX 78712.

This article contains supporting information online at https://www.pnas.org/lookup/suppl/doi:10.1073/pnas.2018140118/-/DCSupplemental.

Published February 1, 2021.

simulated office, and a simulated aircraft cabin (14, 21–23), have all highlighted the importance of the direct presence of human occupants for ozone chemistry. For residences, which are often less densely occupied, evidence is lacking regarding the overall features of indoor ozone chemistry and its impact on the indoor air composition to which occupants are exposed.

Here, we report an investigation of indoor ozone chemistry in a normally occupied residence based on temporally and spatially resolved observations of volatile organic compounds (VOCs) and ozone. Data were acquired in a single-family house in Oakland, California, from an extensive 8-wk monitoring campaign conducted during the summer of 2016 (24, 25). This paper builds on our earlier analysis of the same data set regarding ventilation and airflow patterns in the house (25), as well as concentrations and source characteristics of indoor VOCs (24). In this paper, we examine the spatial and temporal distribution of ozone concentration, estimate the chemical loss rate coefficient of ozone in the living space, characterize the oxidation products of skin oil lipids, and undertake a nontargeted analysis to identify VOC species significantly derived from ozone-initiated chemistry.

Results and Discussion

Ozone in the House. Fig. 1 *Top* presents the diel variation of ozone concentration measured at different locations in the house during the occupied period under the space-resolved measurement scheme (cf. *Materials and Methods*). Mean ozone mixing ratios during the same periods are reported in Table 1. The outdoor ozone level exhibited modest diel variation, with the hourly median peaking at 28 parts per billion by volume (ppb) in the afternoon and declining to 20 ppb in the early morning. The ozone level in different compartments of the house can be understood in the context of the airflow patterns, that is, with air generally flowing upwards from the crawlspace to the living space and then to the attic; downward flows were rare (25). The crawlspace air, coming directly from outdoors through designed vents, exhibited consistently low ozone levels (a mean value of 3.4 ppb), indicating substantial ozone loss in the crawlspace. The loss may be associated with ozone titration by NO emitted from pilot lights of one or both of the natural-gas furnace and water heater installed in the crawlspace; elevated NO was observed in the crawlspace during wintertime monitoring in this house (26). The airflow path into the living space showed a strong diel variation, with 90% of air infiltrating from the ozone-deficient crawlspace at night, whereas 80% directly entered from outdoors in the afternoon through opened windows (Fig. 1, *Bottom*). Correspondingly, the median indoor-to-outdoor (I/O) ratio of ozone varied from 0.12 at night to ~0.27 in the afternoon (Fig. 1, *Middle*). As a point of comparison, previously reported I/O ratios for ozone are typically in the range of 0.2 to 0.7 (6). In the unoccupied (and unfinished) attic, where airflow originated both from the living space and from outdoors, the ozone level was similar to that in the living space, whereas in the small basement room, with a constantly open window, ozone exhibited strong diel variation that was closest to outdoor concentrations in the midafternoon.

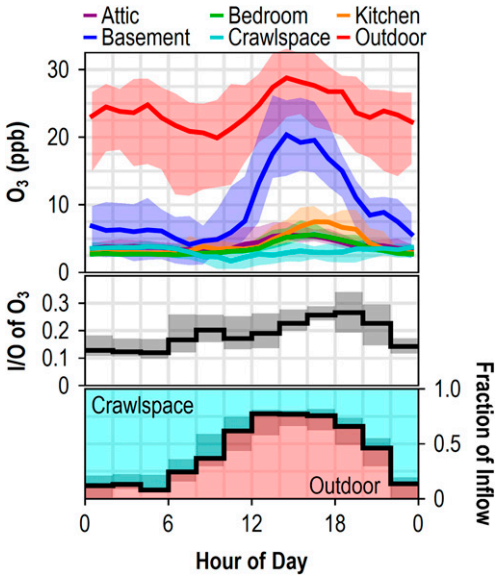

Fig. 1. Diel variation of ozone concentrations in various locations of the studied house (*Top*), indoor ozone concentration in the living space normalized by outdoor concentration (I/O) (*Middle*), and apportionment of air flowing into the living space, between directly from outdoors and via the crawlspace (*Bottom*). Data are shown for normally occupied period averaged during the 5-wk-long space-resolved measurement mode. The solid lines, respectively, represent medians; the shaded regions represent the corresponding interquartile ranges.

The following analysis mainly focuses on the living space where human exposure occurs. The mean ozone level in the living space (indoor ozone) was only 4.3 ppb, at the lower end of reported values for residences in California (27). Assuming a well-mixed living space, the indoor ozone concentration $[O_3]_{in}$ is described well by the following equation:

$$\frac{d[O_3]_{in}}{dt} = \left(f_{crawl}[O_3]_{crawl} + f_{out}[O_3]_{out}\right)ACR - \left(ACR + k_{o_3}\right)[O_3]_{in}, \quad [1]$$

where $[O_3]_{crawl}$ and $[O_3]_{out}$ are the ozone concentrations (in ppb) measured in the crawlspace and outdoors, respectively; f_{crawl} and f_{out} are the fraction of airflow into the living space from the crawlspace and outdoors, respectively; ACR is the air change rate of the living space (h^{-1}); and k_{o_3} is the first-order chemical loss rate coefficient of ozone in the living space (h^{-1}). In Eq. **1**, ozone loss across the building envelope through intended and unintended openings is neglected (28). Rearranging Eq. **1**, we can estimate the overall chemical loss rates of ozone L_{o_3} (ppb/h) as follows:

$$L_{o_3} = k_{o_3}[O_3]_{in} = \left(f_{crawl}[O_3]_{crawl} + f_{out}[O_3]_{out} - [O_3]_{in}\right)ACR - \frac{d[O_3]_{in}}{dt}. \quad [2]$$

For uses of Eq. **2**, ACR, f_{crawl}, and f_{out} were calculated with 2-h resolution, utilizing tracer-gas measurements to determine time-resolved air change rate (25).

The indoor ozone chemical loss rate, L_{o_3}, with 2-h resolution, was obtained for all space-resolved measurement periods. Fig. 2 shows the scatter plot of L_{o_3} versus the ozone concentration $[O_3]_{in}$ in the living space. Given the low ozone level in the crawlspace, data are only shown for $f_{out} > 0.6$ to exclude low-signal values with correspondingly high uncertainty. This emphasizes daytime data. In Fig. 2, the slope from any data point to zero would correspond to its k_{o_3} value ($k_{o_3} = L_{o_3}/[O_3]_{in}$). As shown in Fig. 2, k_{o_3} values of most data points lie within lines corresponding to the range 0.8 to 2.0 h^{-1}, and the overall best-fit k_{o_3} value is 1.3 h^{-1}. These values are at the lower end of reported ozone decay rate coefficients in residences. For example, measured k_{o_3} values varied from 1 h^{-1} to 8 h^{-1} in 43 homes in southern California with mean (± SD) of 2.8 (± 1.3) h^{-1} (2) and varied from 1.3 h^{-1} to 6.0 h^{-1} in 14 residences in China (1). Note that our results were obtained under normal occupancy without manipulating indoor ozone, whereas the cited studies derived k_{o_3} by experimentally elevating ozone and then

Table 1. Summary for ozone concentration and VOC signals identified as having a major origin from indoor ozone chemistry

	VOC signals		Mean mixing ratio[§] (ozone in ppb; VOC signals in ppt)						
	Ion*	Species[†]	Outdoor	Kitchen	Bedroom	Crawlspace	Basement	Attic	Yield[¶]
Ozone			23	4.6	3.8	3.4	9.9	4.5	
PTR	$C_5H_9O_2^+$	4-OPA	39	400	420	56	190	240	2.6%
	$C_8H_{15}O^+$	6-MHO	6	180	190	17	58	94	2.7%
	$C_8H_{13}^+$	6-MHO[‡]	7	160	170	19	59	100	
	$C_8H_{17}O^+$	Octanal	4	120	130	12	31	77	≥0.6%
	$C_9H_{17}O^+$	Nonenal	4	82	85	9	24	44	≥1.0%
	$C_9H_{15}^+$	Nonenal[‡]	5	71	65	9	25	30	
	$C_9H_{19}O^+$	Nonanal	3	370	370	21	98	160	≥3.5%
	$C_9H_{17}^+$	Nonanal[‡]	5	150	150	17	71	67	
	$C_{10}H_{21}O^+$	Decanal	6	200	230	17	87	90	≥1.3%
	$C_{11}H_{23}O^+$	Undecanal	3	45	52	6	20	26	≥0.3%
	$C_{12}H_{25}O^+$	Dodecanal	2	28	32	5	13	15	≥0.2%

*The PTR ions presented here are those well above the baseline in Fig. 5.
[†]Species are attributed by matching identified ion formulas with known indoor ozonolysis products. These species probably make a dominant contribution to corresponding ion signals in the living space but may or may not in other spaces.
[‡]Ratios of two VOC signals attributed to the same species might be slightly different in kitchen and bedroom due to the presence of other minor contributing species.
[§]Mean mixing ratio during occupied period when in space-resolved measurement mode.
[¶]Yield for identified VOC species, estimated as the sum of yields for respective identified product ions. For some species, the sum only represents a lower limit due to the possible presence of unidentified fragment ions (cf. *SI Appendix*).

ENVIRONMENTAL SCIENCES

monitoring its decay under house-closed condition in the absence of occupants. The sustained long-term average ozone loss rate (as measured in our work) might be lower than the short-term loss rate associated with a sudden ozone enhancement (as reported in prior literature).

Ozonolysis Products from Squalene. Next, we explore the VOC data for products arising from indoor ozonolysis. VOC signals were measured using a proton-transfer-reaction (PTR) time-of-flight (ToF) mass spectrometer (MS; see *Materials and Methods*). Our analysis starts by focusing on the unique and most abundant volatile products of squalene ozonolysis: 6-MHO ($C_8H_{14}O$) and 4-OPA ($C_5H_8O_2$). In PTR–MS analysis, 6-MHO is detected as $C_8H_{15}O^+$ and $C_8H_{13}^+$ ions and 4-OPA appears as the $C_5H_9O_2^+$ ion (22). Measured signals of these ions might also have contributions from other isomeric compounds. Below we show that the temporal pattern of indoor $C_8H_{15}O^+$ and $C_5H_9O_2^+$ signals is consistent with the dominant contributions originating from 6-MHO and 4-OPA.

Fig. 3 shows a 1-wk time series of $C_8H_{15}O^+$ and $C_5H_9O_2^+$ ions as well as time series of factors that possibly influence indoor 6-MHO and 4-OPA, including occupancy, air change rates, indoor temperature, and indoor ozone concentration. Signals of both $C_8H_{15}O^+$ and $C_5H_9O_2^+$ ions in the kitchen and bedroom were more than an order of magnitude higher than outdoors, indicating strong indoor sources. A key feature of the time series is that higher indoor signals were typically observed during daytime, when the air change rates and indoor ozone concentrations were higher (e.g., September 20 to 24). Higher air change rate alone is normally expected to reduce indoor concentration of species with a dominant indoor source. The higher ion signals of $C_8H_{15}O^+$ and $C_5H_9O_2^+$ observed in these cases are consistent with theoretical predictions that 6-MHO and 4-OPA production from squalene ozonolysis can outweigh removal by ventilation (29). In particular, when the occupants hosted a party on the evening of September 22, with 17 persons present in the house (and, therefore, substantially more squalene available for ozonolysis), elevated $C_8H_{15}O^+$ and $C_5H_9O_2^+$ signals were observed despite the higher ventilation rate during that event. Additionally, signals of the two ions exhibited sporadic and brief spikes, likely associated with sources other than squalene ozonolysis or other compounds (*SI Appendix*). However, these spikes only represent minor contributions to overall ion signals.

Further analysis is based on net indoor source strengths (S) of VOC signals instead of their concentrations. Utilizing a

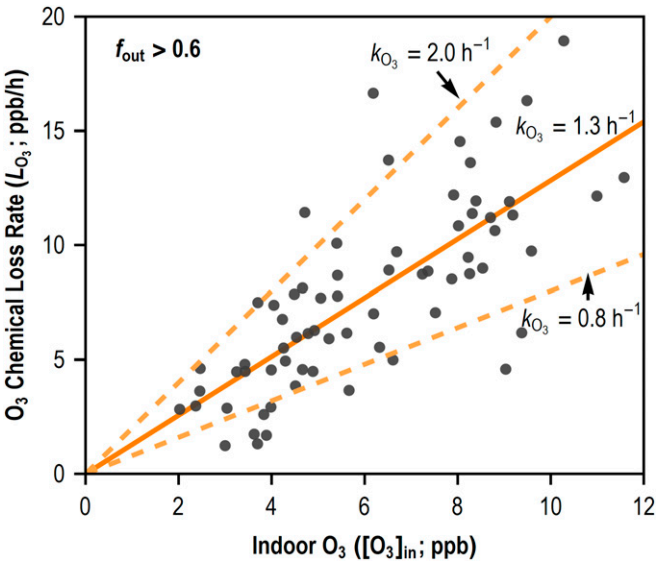

Fig. 2. Scatter plot of the indoor chemical loss rates of ozone Lo_3 (ppb per hour) versus the living-space ozone concentration $[O_3]_{in}$ (ppb). The loss rate, Lo_3, was calculated using Eq. **2** based on the mass balance of ozone in the living space with 2-h resolution. Data are shown for times when the outdoor fraction of total airflow into the living space (f_{out}) is greater than 0.6. The solid orange line represents the best linear fit to the data. Dashed orange lines have slopes of 0.8 and 2.0 h^{-1}, respectively.

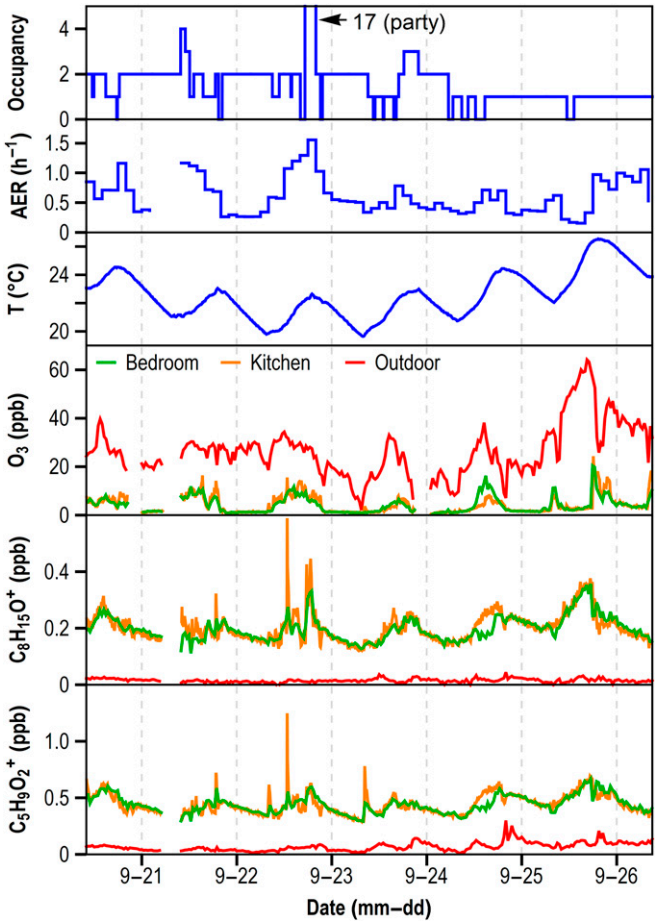

Fig. 3. Time series of VOC signals that might be attributed to products from squalene ozonolysis and possible influencing factors. Panels from top to bottom show occupancy (number of persons present indoors), air change rate (ACR; h^{-1}), indoor temperature (T; °C), ozone concentration (ppb), $C_8H_{15}O^+$ signal (ppb), and $C_5H_9O_2^+$ signal (ppb). $C_8H_{15}O^+$ and $C_5H_9O_2^+$ ions correspond to the pronated ions of 6-MHO ($C_8H_{14}O$) and 4-OPA ($C_5H_8O_2$) without fragmentation, respectively.

mass–balance equation, indoor source strengths of VOC signals (ppb/h) have been determined with 2-h resolution from simultaneously measured air change rates and indoor and outdoor concentrations (24). If the indoor source strength (S_i) of a VOC i is contributed by production (P_i) from ozone chemistry, in addition to direct emission, one can represent the total production rate as $S_i = S_{i,0} + P_i = S_{i,0} + k_i\,[O_3]_{in}$, where $S_{i,0}$ is the ozone-independent emission rate of i (ppb/h) and k_i is an effective first-order production rate coefficient of i from ozone reaction (h^{-1}). In the case that squalene ozonolysis is the dominant reaction to produce i, k_i would be proportional to the amount of squalene indoors available for reaction. Note that this equation is a simplified representation; the determined S_i is a net value, incorporating not only indoor emission and chemical production but also indoor wall interaction and possible indoor loss from chemical reaction.

Fig. 4*A* shows the dependence of source strength of the $C_8H_{15}O^+$ ion on indoor ozone concentration $[O_3]_{in}$ with data points colored by occupancy. Fig. 4*A* includes all available data subject to the constraint that indoor temperature is restricted to the range 20.5 to 23.5 °C to minimize possible confounding effects of temperature (*SI Appendix*, Fig. S1). As shown in Fig. 4*A*, $C_8H_{15}O^+$ source strength exhibits close correlation with indoor ozone. The R^2 of a linear fit of the data set after excluding two outliers (source strength greater than upper quartile plus 3× interquartile range) is 0.66. The fitted slope, corresponding to the production rate coefficient of $C_8H_{15}O^+$ from first-order ozone reaction (k), is 0.018 h^{-1}. The fitted intercept, corresponding to ozone-independent baseline emission rate (S_0), is 0.0072 ppb/h. A striking feature in Fig. 4*A* is that the baseline emission S_0 (intercept) was small compared with the range of ozone-dependent production $k[O_3]_{in}$ (e.g., an increase by 0.18 ppb/h for 10 ppb of indoor ozone). This feature quantitatively demonstrates that 6-MHO production from ozone chemistry was the dominant source of measured $C_8H_{15}O^+$ signals. A similarly strong dependence of source strength on ozone was also found for $C_8H_{13}^+$ (the other product ion of 6-MHO) and $C_5H_9O_2^+$ (4-OPA), as presented in *SI Appendix*, Fig. S2.

Fig. 4*A* also explores the role of occupancy. Since only two adults lived in the house, two or fewer persons were typically

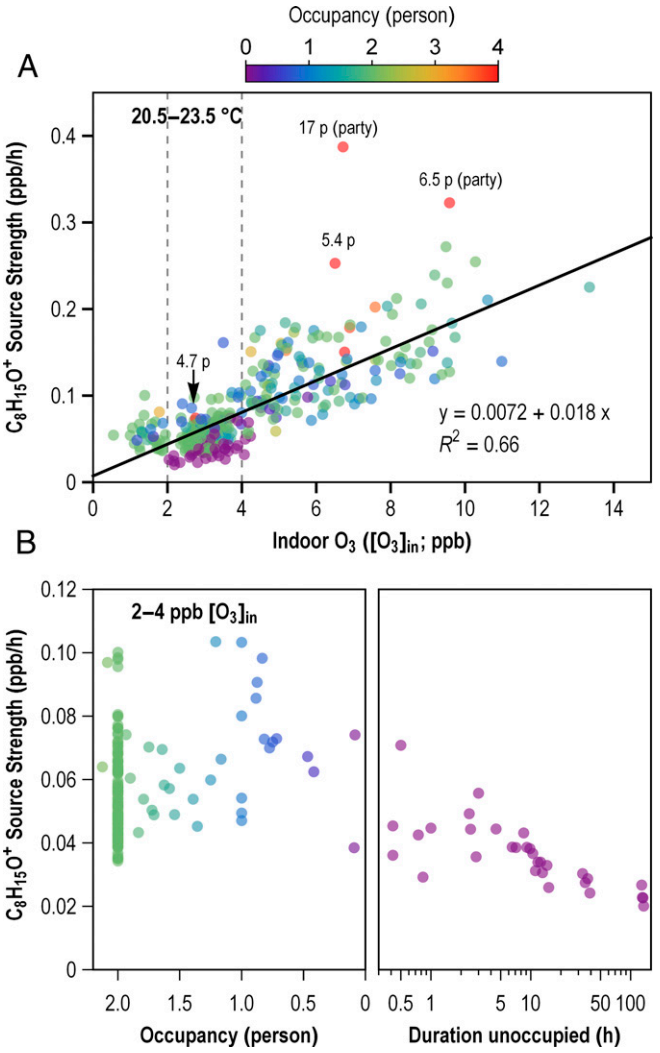

Fig. 4. Dependence of $C_8H_{15}O^+$ (6-MHO) source strength on (*A*) indoor ozone concentration and (*B*) occupancy. (*A*) shows all available data using 2-h resolution and restricted to an indoor temperature range of 20.5 to 23.5 °C. (*B*) uses a subset of data in *A* (bounded by dashed lines, with indoor ozone of 2 to 4 ppb) and plots $C_8H_{15}O^+$ source strength versus occupancy for 2 ≥ occupancy > 0 (*Left*) and versus unoccupied time duration for occupancy = 0 (*Right*), respectively. Data points are colored to indicate occupancy level. In *A*, the black line shows a linear fit of data after excluding outliers of $C_8H_{15}O^+$ source strength (greater than upper quartile plus 3× interquartile range); exact occupancy level was labeled for occupancy >4. Occupancy level represents the average for the 2-h integration period and so can be a noninteger value when occupants are present for only part of the interval.

present in the living space, with some exceptions due to visits of guests (particularly during the party). Data for the presence of more than four persons are labeled in Fig. 4*A*. Although there were only four such points, they each lie above the general trend line. Such occupancy dependence is consistent with expectations for squalene ozonolysis: more people present in the house would mean more squalene available for ozone reaction, leading to a larger k value. The role of occupancy is also evident in the spatial distribution of ozone oxidation products associated with squalene. Table 1 shows that ions associated with 6-MHO and 4-OPA were much higher in the routinely occupied spaces (kitchen and bedroom) than in rarely occupied auxiliary spaces (crawlspace and attic). Given the regular movement of air from the kitchen and bedroom to attic, it is reasonable that the concentrations in the attic were higher than those in the crawlspace. A comparison of basement and crawlspace levels is also informative. The basement exhibited the highest level of ozone (Fig. 1) and also was a site for a clothes washer and soiled laundry; the crawlspace was never occupied and did not contain clothing or other objects associated with occupant contact. The $C_8H_{15}O^+$ signal was much higher in the basement than in the crawlspace.

Fig. 4*B* explores the role of occupancy for cases with a low occupancy level by analyzing a subset of data from Fig. 4*A* with indoor ozone concentration restricted to the range 2 to 4 ppb. This ozone range was chosen because it covered most data points during periods with zero occupancy. Fig. 4*B* plots the source strength of $C_8H_{15}O^+$ signals as a function of occupancy (left frame for $0 <$ occupancy ≤ 2 persons) and then the elapsed time since the house was last occupied (right frame for occupancy = 0). From the left frame, one cannot clearly discern how $C_8H_{15}O^+$ source strength changed with occupancy level given the variability of the data. For periods with between one and two occupants, the source strength averaged 0.056 ppb/h with a SD of 0.014 ppb/h. However, when the house was unoccupied (right frame), $C_8H_{15}O^+$ source strength slowly decreased with the duration of vacancy. The source strength was about 0.045 ± 0.016 ppb/h when the house was unoccupied for less than 1 h and diminished by about half, to 0.023 ± 0.003 ppb/h, when the unoccupied period of time increased to ~130 h. Given that the reaction between ozone and 6-MHO is fast [second-order rate coefficient of 3.9×10^{-16} $cm^3 \cdot mol^{-1} \cdot s^{-1}$ (30)], along with the small intercept in Fig. 4*A* (baseline emission level of 0.007 ppb/h), it is unlikely that surface reservoirs were a substantial source of 6-MHO during the unoccupied period. Instead, the more probable explanation is that ozone reacted with squalene in skin flakes and skin oils that had accumulated on exposed surfaces in the home. Assuming that this interpretation is correct, we can further infer that during normal occupancy (Fig. 4 *B*, *Left*), the contribution of off-body skin oil/flakes to $C_8H_{15}O^+$ source strength (~0.045 ppb/h, estimated as the level during initial unoccupied period) was substantially larger than the contribution from the body envelopes of the occupants (~0.011 ppb/h, estimated as the difference of 0.056 ppb/h and 0.045 ppb/h).

This evidence contains a clue to help reconcile the apparent contradiction between the elevation of $C_8H_{15}O^+$ source strength in the presence of >4 persons (Fig. 4*A*) and the absence of any source-strength dependence on occupancy level under the normally low occupancy (Fig. 4 *B*, *Left*). That is, the off-body squalene contributes substantially to the total squalene-associated ozone reactivity when the house is normally occupied by two (or fewer) occupants, such that the influence of occupancy changes is attenuated. With this interpretation, the contribution of on-body squalene became substantial only in the rare presence (during this monitoring campaign) of multiple guests.

The large contribution of off-body skin oils is also consistent with high effective yields of 6-MHO and 4-OPA in this study. The effective yields of 6-MHO and 4-OPA (Table 1) were estimated by taking the ratio of the total production rate coefficient $\sum k_i$ of corresponding identified VOC signals (slope in Fig. 4*A* and *SI Appendix*, Fig. S2) to the chemical loss-rate coefficient of ozone, k_{O_3} (Fig. 2); that is, $y_i = \sum k_i / k_{O_3}$. By definition, the obtained effective yields are relative to the total ozone loss in the house on a molecular basis and provide overall characterization of indoor ozone chemistry without differentiating among organic/inorganic precursors, primary/secondary reactions, or heterogeneous/gas-phase reactions. That said, we expect most surfaces to be covered with thin films that result from the accumulation over time of semivolatile organic compounds and airborne particles (4, 31, 32). The house where the sampling occurred was built in the 1930s, and there had been no recent renovation or refurnishing of note. As has been demonstrated for freshly cleaned windows (33) and vertically positioned glass capillary tubes (34), organic surface films with thicknesses on the order of 10 to 20 nm accumulate over months in typical indoor environments. In the studied house of volume 350 m^3 (floor area ~140 m^2) normally occupied by two adults, the combined effective yield of 6-MHO and 4-OPA was 5.2% per consumed ozone, on a molecule-by-molecule basis. Remarkably, this combined yield is as high as that reported for a simulated aircraft cabin of 28.4 m^3 in the presence of 16 subjects (22). The simulated aircraft was only occupied during the experiments and was unlikely to have been widely soiled with skin flakes and skin oils to the extent that an occupied home would be. Although other factors might also come into play, substantial soiling by skin flakes and skin oils could help reconcile the observed high yield of squalene oxidation products despite the low occupant density in this study.

A contribution to ozone reactivity from off-body skin flakes/oil has been anticipated (18, 35) and is supported by recent studies (4, 32). The magnitude of this contribution compared to that of on-body squalene revealed herein is potentially surprising. However, upon closer examination, the result seems reasonable. Two humans in 350 m^3 of living space are estimated to remove ozone with a first-order rate constant of ~0.2 h^{-1} (18), which accounted for about one-sixth of the central tendency for k_{O_3} in Fig. 2 (1.3 h^{-1}). While we do not know the contribution to k_{O_3} of skin flakes and skin oils accumulated on "off-body" surfaces, circumstantial evidence indicates that it is significant. Humans shed their entire outer layer of skin every 2 to 4 wk (36). In dust samples collected from 500 children's bedrooms in Odense, Denmark, squalene was the third-most-abundant identified organic, with a median mass fraction of 32 μg/g (35). Squalene is semivolatile, with a vapor pressure of 3.7×10^{-7} Pa at 25 °C (37), and so sorption to indoor surfaces via gas-phase transport may also occur. Furthermore, the low level of indoor ozone at the residence that we studied might contribute to the accumulation of off-body squalene since the persistence time scale of squalene should be longer with slower ozonolysis. As a related point, Deming and Ziemann recently reported an observation of ubiquitous C = C bonds in surface films on various indoor surfaces in a classroom and proposed that human skin lipids could be a major source (4). Based on decrease of 6-MHO source strength during the vacant period, we roughly estimated the lifetime of off-body squalene was ~400 h and the total amount of off-body squalene present was ~0.36 mmol (equal to 150 mg) (*SI Appendix*). The associated surface C = C concentration would be ~2 μmol/m^2, largely consistent with the observations of Deming and Ziemann (4).

Previous indoor studies in simulated microenvironments as well as in a classroom have highlighted the importance of ozone reactions with on-body squalene (14, 21, 22). The current study identifies a substantial contribution of off-body skin lipids to ozone chemistry in a normally occupied residence. This finding merits further investigation. Contributions of off-body skin oils might also influence densely occupied environments, in addition to residences. For example, Tang et al. estimated occupant and

nonoccupant VOC source strengths in a university classroom in California (38). Their results indicated a nonoccupant source strength of about 25% of the occupant source for 6-MHO and about 80% for 4-OPA. It is plausible that these contributions resulted from ozonolysis of off-body squalene that originated from skin oils and skin flakes of classroom occupants. Additionally, our results call for caution in extrapolating simulated scenarios of ozone chemistry in test houses or chambers. That is, because such facilities are not routinely occupied, they lack an important element of real-world settings—soiling of indoor surfaces by the skin oil and skin flakes of occupants.

Nontargeted Analysis of Ozonolysis Products. To explore whether other indoor VOCs might be substantially associated with ozonolysis, we developed and applied a systematic screening approach. As a screening index, we computed a dimensionless source strength ratio, defined as the increase in source strength for a fixed increment (10 ppb) of ozone concentration ($\Delta S_{10\text{ppb}O_3}$) divided by the baseline source strength (S_0). A higher value of $\Delta S_{10\text{ppb}O_3}/S_0$ indicates a larger contribution of ozone chemistry to the overall VOC signal. As illustrated in Fig. 4*A*, this index can be obtained from the linear fit of indoor source strength of a VOC signal versus indoor ozone over a restricted indoor temperature range (20.5 to 23.5 °C) and after removing extreme outliers, where S_0 corresponds to the fitted intercept and $\Delta S_{10\text{ppb}O_3}$ is extracted from the fitted slope.

A confounding factor in the evaluation of this index is ventilation. Due to the effects of indoor surface reservoirs, an increase of ventilation rate was associated with a less-than-anticipated decrease of indoor VOC signals (39, 40) and, hence, an apparent increase of net source strength (*SI Appendix*, Fig. S3). Considering that indoor ozone levels tended to be higher with higher ventilation rates (Fig. 3), this effect can create a correlation between indoor source strength and ozone, even for compounds whose constituents do not have oxygen and therefore clearly did not arise directly from ozonolysis (*SI Appendix*, Fig. S3). To compensate, we compute a supplementary index, the concentration ratio of a species at two air change rates—1 h^{-1} and 0.25 h^{-1} ($C_{1h^{-1}}/C_{0.25h^{-1}}$)—which is an indicator of the surface-reservoir effect. Values of this index for VOC signals were obtained from linear fits of indoor–outdoor concentration difference versus air change rate at 20.5 to 23.5 °C, after removing outliers.

Fig. 5 shows a scatter plot of $\Delta S_{10\text{ppb}O_3}/S_0$ versus $C_{1h^{-1}}/C_{0.25h^{-1}}$ for 61 VOC signals that feature continuous indoor sources. These signals were selected based on the same criteria as in our previous paper, excluding those that have either strong influence from intermittent emissions (such as cooking) or considerable contributions from outdoors or crawlspace air (24). Each data point represents a VOC signal. The color indicates the R^2 of the linear fit of its source strength versus indoor ozone. The point size scales with the fitted slope. Values of $C_{1h^{-1}}/C_{0.25h^{-1}}$ ranged from 0.45 to 1.37, much higher than the value of 0.25 that would be expected for a constant source strength case, with no wall effects, and for steady-state conditions. Values of $\Delta S_{10\text{ppb}O_3}/S_0$ ranged from 0.6 to 26.

Most data points in Fig. 5 are distributed along a line with a positive slope; other points lie above the line. The line represents a lower bound of $\Delta S_{10\text{ppb}O_3}/S_0$ for a given $C_{1h^{-1}}/C_{0.25h^{-1}}$, likely corresponding to the extent of $\Delta S_{10\text{ppb}O_3}/S_0$ that can be explained by surface reservoir effects. This interpretation is supported by two observations. Firstly, the data points generally are aligned with expected stickiness of parent compounds. Specifically, the lowest five points correspond to relatively high volatility species—$C_3H_4N^+$, $C_5H_5O_2^+$, $C_3H_5O^+$, CH_3O^+, and CH_5O^+—whereas the highest five are for species with lower volatility—$C_{15}H_{27}N_2^+$, $C_9H_{15}O_2^+$, $C_7H_{11}O^+$, $C_{15}H_{23}^+$, and $C_8H_{17}O_2^+$. Secondly, all values of $C_{1h^{-1}}/C_{0.25h^{-1}}$ on the line are

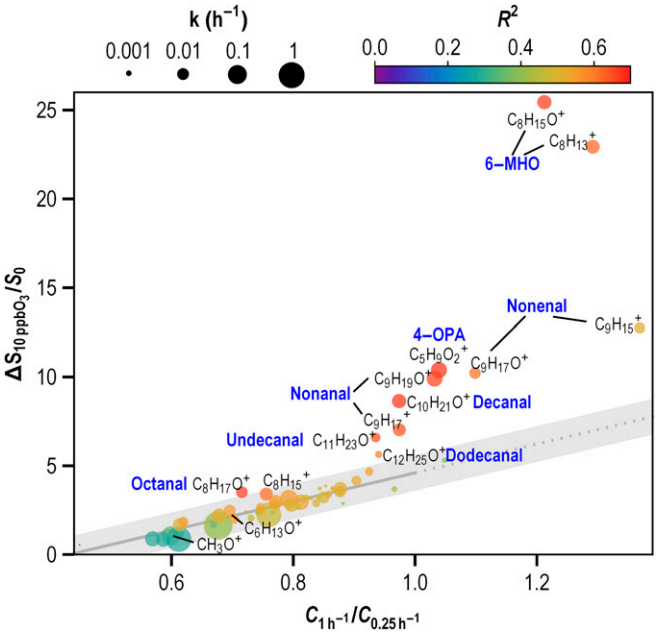

Fig. 5. VOC signals for continuously emitted species mapped into a two-dimensional plot to identify compounds with pronounced production from indoor ozone chemistry. The *y* axis is indoor source strength ratio, defined as change of source strength associated with a 10-ppb increase of ozone, normalized by the ozone-independent source strength ($\Delta S_{10\text{ppb}O_3}/S_0$); and the *x* axis is an indoor concentration ratio, defined as concentration at an air change rate of 1 h^{-1} divided by that at 0.25 h^{-1} ($C_{1h^{-1}}/C_{0.25h^{-1}}$). Each data point is colored by R^2 of the linear fit of indoor source strength versus indoor ozone, and the point size is scaled to the corresponding slope (*k*). The gray line represents a fit to the baseline. Emissions for chemicals along this line are ozone independent. The light gray region represents an approximate uncertainty band, plotted as the line value ± 1.

less than 1.0 (solid line), consistent with expectation from a surface reservoir effect, which can make indoor species concentration at the higher air change rate close to, but no more than (dotted line), that at the lower air change rate.

Based on the above analysis, we can consider that the VOC signals for points situated well above the line in Fig. 5 are strongly produced by ozone chemistry. Among these VOC signals, $C_8H_{15}O^+$ and $C_8H_{13}^+$ attributed to 6-MHO exhibited a notably high $\Delta S_{10\text{ppb}O_3}/S_0$ value above 20. Other VOC signals well above the line (i.e., above the gray region) include $C_5H_9O_2^+$ attributable to 4-OPA, $C_9H_{17}O^+$ and $C_9H_{15}^+$ attributable to nonenal, and ions attributable to the C_8-C_{12} saturated aldehdyes. As presented in Table 1, the total effective yield for all identified compounds is at least 12%. The effective yield of nonanal was the highest (≥3.5%), followed by 6-MHO (2.7%), 4-OPA (2.6%), decanal (≥1.3%), and nonenal (≥1.0%). Note that, except for 6-MHO and 4-OPA, the estimated yields represent lower limits, since our analysis might have missed some smaller fragment ions of these aldehydes (*SI Appendix*). The identified compounds, with summed indoor concentration of several parts per billion, contribute only marginally to the total loading of oxygenated VOCs in this house, which was several hundred parts per billion (24). However, certain products may contribute even at low abundances to odors [e.g., nonenal (41)] or irritation [e.g., 4-OPA (42)].

Volatile products identified through this nontarget analysis are among the most commonly reported products from ozone interaction with indoor surfaces and human skin oil. The C8-C10 aldehydes, particularly nonanal, have been reported as key products of ozonolysis for many indoor building and furnishing

materials (9–11, 15). Surface soiling by omega-9 fatty acids/esters from cooking oil might lead to additional nonanal production, as suggested by field measurements (8, 16), as well as by laboratory tests of building materials placed in real indoor environments (17). Notably, Wang and Morrison found that nonanal was the most prominent secondary aldehyde emitted from almost all the tested surfaces in residences they studied (8, 16); the product yield varied in the range 0 to 34% across the surfaces sampled. Their observation is consistent with our finding that nonanal exhibited the highest effective yield of ≥3.5% among all identified products. For ozone interaction with skin lipids, decanal is another key oxidation product in addition to 6-MHO and 4-OPA, specifically from ozonolysis of some abundant unsaturated fatty acids such as cis-hexadec-6-enoic acid (5 to 6% of skin surface lipids by weight) (18). In terms of relative ratios, yields of the three compounds quantified herein (2.7% [6-MHO]:2.6% [4-OPA]:≥1.3% [decanal]) are comparable with those reported in a simulated office experiment for skin oil ozonolysis with two occupants (14.4% [6-MHO]:12.5% [4-OPA]:6.3% [decanal]) (14). Octanal, undecanal, and dodecanal were also detected in skin oil ozonolysis experiments, but their fatty acid precursors are less abundant (14).

The unsaturated aldehyde nonenal has been previously identified as an oxidation product of new carpets (2-nonenal) (11, 16), certain skin surface lipids (3-nonenal) (18), omega-7 unsaturated fatty acids (2-nonenal) (43), and linoleic acid (2- and 4-nonenal) (44), a common constituent of linseed oil and certain cooking oils. In the house we studied, there were older area carpets in several rooms, and cooking activities occurred frequently. We cannot glean from the evidence which precursor(s) contributed to the secondary production of nonenal. Worth noting is that nonenal was not detected in previous field measurements on kitchen countertops where nonanal was prominent (8, 16). However, we suspect that result might be a technical artifact arising from the off-line analysis method used in those studies. That is, nonenal, which contains a C = C bond, might have been consumed by ozone reaction after collection on Tenax tubes, considering the use of a high level of ozone (40 to 120 ppb) and the absence of an ozone scrubber during sampling. In any case, given the high yield of nonenal observed here, in combination with the particularly low odor threshold for this compound (41), further investigation of nonenal from indoor ozonolysis reactions is warranted.

It should be noted that some frequently reported ozonolysis products in previous studies of indoor surfaces or skin oil, including formaldehyde, acetone, hexanal, and geranylacetone, did not emerge as apparent ozone byproducts in our analysis (Fig. 5). Ions corresponding to formaldehyde (CH_3O^+) and hexanal ($C_6H_{13}O^+$) lie near the baseline in Fig. 5, suggesting no more than a marginal contribution of ozone chemistry to indoor formaldehyde and hexanal generation. Major indoor sources of formaldehyde include urea-formaldehyde-bonded composite wood products (45). Continuous indoor sources of hexanal are uncertain but may be related to certain wood materials (46, 47). Acetone was excluded from the analysis in Fig. 5, because of strong contributions from intermittent sources as indicated by a high mean-to-median concentration ratio (24). Sources of acetone include human breath and household cleaning agents. The yield of acetone has been reported to be about 2 times higher than 6-MHO for skin oil ozonolysis (14), but the measured indoor concentration of acetone in the present study was 50 times higher than of 6-MHO, suggesting that the contribution of ozone chemistry for acetone at this site was relatively small. Geranylacetone was also excluded in Fig. 5, because its indoor-to-outdoor ratio (indicator for strong indoor source) and mean-to-median ratio did not reach the selection criteria. Even if we relax the data constraint to include the product ion of geranylacetone in the analysis (*SI Appendix*, Fig. S4), the ion lies in the gray region and is characterized by a high value of $C_{1h^{-1}}/C_{0.25h^{-1}}$. A probable interpretation is that the stickiness of geranylacetone to indoor surfaces strongly interferes with our ability to discern its relationship to ozone-initiated chemistry using our approach. Given the presence of these and other compounds which can be contributed by ozone chemistry but did not emerge as apparent ozone byproducts, the actual total yield of volatile organic products from ozone chemistry in the house can be several times higher than the summed effective yield of all identified compounds reported here.

To summarize, the results presented in this paper represent a quantitative characterization of ozone-initiated chemistry in a normally occupied residence. We identified a range of VOCs that had strong contributions from indoor ozone chemistry (Fig. 5), even though the house we studied had both low indoor ozone concentrations (Fig. 1) and a low indoor ozone loss rate (Fig. 2). Being able to elucidate how residential VOC composition is altered by ozone-initiated chemistry substantiates prior laboratory-based investigations. It is important to recognize that the health effects associated with ambient ozone might be materially influenced by the products of indoor ozone chemistry. Of concern in this regard are not only those species characterized here but also other potentially toxic products known to be a consequence of ozonolysis but which our instrumentation is incapable of detecting, such as secondary ozonides, hydroperoxides, and epoxides (48, 49).

Materials and Methods

The studied house, built in the 1930s of wood-frame construction, has a split-level living zone, an unoccupied attic above, and a small basement and larger crawlspace below. Two adult occupants (male and female, aged 60 to 65 y) live in the house. In addition to normal house operation conditions (occupied periods), the occupants were deliberately away on a few occasions for one or more days during the monitoring period. During the vacant periods, the house windows and exterior doors were closed. Other than a request to maintain interior doors open (to facilitate interzonal transport and mixing), occupants were instructed to live as they normally would, including normal use of window opening to maintain thermal comfort. The occupants gave informed consent for this study, which was approved by the Committee for Protection of Human Subjects for the University of California, Berkeley (Protocol #2016-04-8656).

Ozone and VOCs were measured using an ultraviolet (UV) absorption–based ozone monitor (Thermal 49i) and a PTR–ToF–MS, respectively. Both instruments were situated in a detached garage and subsampled via shared continuous-operating equal length 30-m perfluoroalkoxy-alkane sampling lines from the kitchen, bedroom, crawlspace, basement, attic, and outdoors. During vacant periods, sampling was conducted using a spaced-resolved scheme (sampling from each of the six locations for 5 min in a twice-per-hour cycle). During occupied periods, sampling was conducted using the space-resolved measurement scheme for ∼5 wk and using a time-resolved scheme (outdoor 5 min, kitchen 20 min, and bedroom 5 min, twice per hour) for ∼2 wk. *SI Appendix* provides a detailed description of the sampling system and associated data trimming protocols, as well as an evaluation of the influence of the sampling system on instrument response.

For PTR–ToF–MS, the primary reagent is the hydronium ion (H_3O^+), which can effectively protonate most oxygenated VOCs. Resultant product ions were measured, often in the form of $VOCH^+$, but fragmentation can also occur. In total, 218 VOC signals (organic ion formulas after combining isotopic ions and some known fragment ions) were extracted to represent measured VOC speciation across the campaign (24). Depending on sample air composition, a VOC signal might be dominantly attributed to one VOC species and might be contributed by a few species. Airborne concentrations (in part per trillion/billion by volume; ppt/ppb) were estimated for individual VOC signals as described in *SI Appendix*.

Data associated with this paper are provided in Dataset S1.

Data Availability. All study data are included in the article and supporting information.

ACKNOWLEDGMENTS. This work was funded by the Alfred P. Sloan Foundation via Grants 2016-7050 and 2019-11412. Y.L. acknowledges support from an Alfred P. Sloan Foundation Postdoctoral Fellowship (Grant 2015-14166) and support by the 111 Project (Grant B20009). We thank occupants in the studied house for volunteering their house and facilitating the measurements. We thank Jianyin Xiong, Yilin Tian, and Robin Weber for their contribution to the field campaign.

1. M. Yao, B. Zhao, Surface removal rate of ozone in residences in China. *Build. Environ.* **142**, 101–106 (2018).
2. K. Lee, J. Vallarino, T. Dumyahn, H. Özkaynak, J. D. Spengler, Ozone decay rates in residences. *J. Air Waste Manag. Assoc.* **49**, 1238–1244 (1999).
3. C. J. Weschler, Ozone's impact on public health: Contributions from indoor exposures to ozone and products of ozone-initiated chemistry. *Environ. Health Perspect.* **114**, 1489–1496 (2006).
4. B. L. Deming, P. J. Ziemann, Quantification of alkenes on indoor surfaces and implications for chemical sources and sinks. *Indoor Air* **30**, 914–924 (2020).
5. J. Shen, Z. Gao, Ozone removal on building material surface: A literature review. *Build. Environ.* **134**, 205–217 (2018).
6. C. J. Weschler, Ozone in indoor environments: Concentration and chemistry. *Indoor Air* **10**, 269–288 (2000).
7. C. Chen, B. Zhao, C. J. Weschler, Assessing the influence of indoor exposure to "outdoor ozone" on the relationship between ozone and short-term mortality in U.S. communities. *Environ. Health Perspect.* **120**, 235–240 (2012).
8. H. Wang, G. Morrison, Ozone-surface reactions in five homes: Surface reaction probabilities, aldehyde yields, and trends. *Indoor Air* **20**, 224–234 (2010).
9. M. Nicolas, O. Ramalho, F. Maupetit, Reactions between ozone and building products: Impact on primary and secondary emissions. *Atmos. Environ.* **41**, 3129–3138 (2007).
10. S. P. Lamble, R. L. Corsi, G. C. Morrison, Ozone deposition velocities, reaction probabilities and product yields for green building materials. *Atmos. Environ.* **45**, 6965–6972 (2011).
11. G. C. Morrison, W. W. Nazaroff, Ozone interactions with carpet: Secondary emissions of aldehydes. *Environ. Sci. Technol.* **36**, 2185–2192 (2002).
12. L. S. Pandrangi, G. C. Morrison, Ozone interactions with human hair: Ozone uptake rates and product formation. *Atmos. Environ.* **42**, 5079–5089 (2008).
13. B. K. Coleman, H. Destaillats, A. T. Hodgson, W. W. Nazaroff, Ozone consumption and volatile byproduct formation from surface reactions with aircraft cabin materials and clothing fabrics. *Atmos. Environ.* **42**, 642–654 (2008).
14. A. Wisthaler, C. J. Weschler, Reactions of ozone with human skin lipids: Sources of carbonyls, dicarbonyls, and hydroxycarbonyls in indoor air. *Proc. Natl. Acad. Sci. U.S.A.* **107**, 6568–6575 (2010).
15. O. A. Abbass, D. J. Sailor, E. T. Gall, Effect of fiber material on ozone removal and carbonyl production from carpets. *Atmos. Environ.* **148**, 42–48 (2017).
16. H. Wang, G. C. Morrison, Ozone-initiated secondary emission rates of aldehydes from indoor surfaces in four homes. *Environ. Sci. Technol.* **40**, 5263–5268 (2006).
17. C. J. Cros, G. C. Morrison, J. A. Siegel, R. L. Corsi, Long-term performance of passive materials for removal of ozone from indoor air. *Indoor Air* **22**, 43–53 (2012).
18. C. J. Weschler, Roles of the human occupant in indoor chemistry. *Indoor Air* **26**, 6–24 (2016).
19. M. Kruza, A. C. Lewis, G. C. Morrison, N. Carslaw, Impact of surface ozone interactions on indoor air chemistry: A modeling study. *Indoor Air* **27**, 1001–1011 (2017).
20. P. Wolkoff, Volatile organic compounds–Sources, measurements, emissions, and the impact on indoor air quality. *Indoor Air* **5 (Suppl. 3)**, 9–73 (1995).
21. J. Xiong, Z. He, X. Tang, P. K. Misztal, A. H. Goldstein, Modeling the time-dependent concentrations of primary and secondary reaction products of ozone with squalene in a university classroom. *Environ. Sci. Technol.* **53**, 8262–8270 (2019).
22. C. J. Weschler *et al*., Ozone-initiated chemistry in an occupied simulated aircraft cabin. *Environ. Sci. Technol.* **41**, 6177–6184 (2007).
23. A. Fischer, E. Ljungström, S. Langer, Ozone removal by occupants in a classroom. *Atmos. Environ.* **81**, 11–17 (2013).
24. Y. Liu *et al*., Characterizing sources and emissions of volatile organic compounds in a northern California residence using space- and time-resolved measurements. *Indoor Air* **29**, 630–644 (2019).
25. Y. Liu *et al*., Detailed investigation of ventilation rates and airflow patterns in a northern California residence. *Indoor Air* **28**, 572–584 (2018).
26. C. Arata *et al*., Measurement of NO_3 and N_2O_5 in a residential kitchen. *Environ. Sci. Technol. Lett.* **5**, 595–599 (2018).
27. K. Lee *et al*., Nitrous acid, nitrogen dioxide, and ozone concentrations in residential environments. *Environ. Health Perspect.* **110**, 145–149 (2002).
28. H. Zhao, B. Stephens, A method to measure the ozone penetration factor in residences under infiltration conditions: Application in a multifamily apartment unit. *Indoor Air* **26**, 571–581 (2016).
29. C. M. Salvador *et al*., Indoor ozone/human chemistry and ventilation strategies. *Indoor Air* **29**, 913–925 (2019).
30. E. Grosjean, D. Grosjean, J. H. Seinfeld, Gas-phase reaction of ozone with trans-2-hexenal, trans-2-hexenyl acetate, ethylvinyl ketone, and 6-methyl-5-hepten-2-one. *Int. J. Chem. Kinet.* **28**, 373–382 (1996).
31. C. J. Weschler, W. W. Nazaroff, Growth of organic films on indoor surfaces. *Indoor Air* **27**, 1101–1112 (2017).
32. E. T. Gall, D. Rim, Mass accretion and ozone reactivity of idealized indoor surfaces in mechanically or naturally ventilated indoor environments. *Build. Environ.* **138**, 89–97 (2018).
33. C.-Y. Huo *et al*., Phthalate esters in indoor window films in a northeastern Chinese urban center: Film growth and implications for human exposure. *Environ. Sci. Technol.* **50**, 7743–7751 (2016).
34. C. Y. Lim, J. P. Abbatt, Chemical composition, spatial homogeneity, and growth of indoor surface films. *Environ. Sci. Technol.* **54**, 14372–14379 (2020).
35. C. J. Weschler *et al*., Squalene and cholesterol in dust from Danish homes and daycare centers. *Environ. Sci. Technol.* **45**, 3872–3879 (2011).
36. H. Baker, A. M. Kligman, Technique for estimating turnover time of human stratum corneum. *Arch. Dermatol.* **95**, 408–411 (1967).
37. A. Zafar, J. Chickos, The vapor pressure and vaporization enthalpy of squalene and squalane by correlation gas chromatography. *J. Chem. Thermodyn.* **135**, 192–197 (2019).
38. X. Tang, P. K. Misztal, W. W. Nazaroff, A. H. Goldstein, Volatile organic compound emissions from humans indoors. *Environ. Sci. Technol.* **50**, 12686–12694 (2016).
39. C. Fortenberry *et al*., Analysis of indoor particles and gases and their evolution with natural ventilation. *Indoor Air* **29**, 761–779 (2019).
40. C. Wang *et al*., Surface reservoirs dominate dynamic gas-surface partitioning of many indoor air constituents. *Sci. Adv.* **6**, eaay8973 (2020).
41. D. G. Guadagni, R. G. Buttery, S. Okano, Odour thresholds of some organic compounds associated with food flavours. *J. Sci. Food Agric.* **14**, 761–765 (1963).
42. S. E. Anderson *et al*., Irritancy and allergic responses induced by exposure to the indoor air chemical 4-oxopentanal. *Toxicol. Sci.* **127**, 371–381 (2012).
43. S. Haze *et al*., 2-Nonenal newly found in human body odor tends to increase with aging. *J. Invest. Dermatol.* **116**, 520–524 (2001).
44. T. Moise, Y. Rudich, Reactive uptake of ozone by aerosol-associated unsaturated fatty acids: Kinetics, mechanism, and products. *J. Phys. Chem. A* **106**, 6469–6476 (2002).
45. T. Salthammer, S. Mentese, R. Marutzky, Formaldehyde in the indoor environment. *Chem. Rev.* **110**, 2536–2572 (2010).
46. A.-M. Manninen, P. Pasanen, J. K. Holopainen, Comparing the VOC emissions between air-dried and heat-treated Scots pine wood. *Atmos. Environ.* **36**, 1763–1768 (2002).
47. A. T. Hodgson, A. F. Rudd, D. Beal, S. Chandra, Volatile organic compound concentrations and emission rates in new manufactured and site-built houses. *Indoor Air* **10**, 178–192 (2000).
48. S. Zhou, M. W. Forbes, J. P. D. Abbatt, Kinetics and products from heterogeneous oxidation of squalene with ozone. *Environ. Sci. Technol.* **50**, 11688–11697 (2016).
49. M. Yao, C. J. Weschler, B. Zhao, L. Zhang, R. Ma, Breathing-rate adjusted population exposure to ozone and its oxidation products in 333 cities in China. *Environ. Int.* **138**, 105617 (2020).